



PEARL

Decreased motility of flagellated microalgae long-term acclimated to CO₂-induced acidified waters

Wang, Yitao; Fan, Xiao; Gao, Guang; Beardall, John; Inaba, Kazuo; Hall-Spencer, Jason M.; Xu, Dong; Zhang, Xiaowen; Han, Wentao; McMinn, Andrew; Ye, Naihao

Published in:

Nature Climate Change

DOI:

[10.1038/s41558-020-0776-2](https://doi.org/10.1038/s41558-020-0776-2)

Publication date:

2020

Link:

[Link to publication in PEARL](#)

Citation for published version (APA):

Wang, Y., Fan, X., Gao, G., Beardall, J., Inaba, K., Hall-Spencer, J. M., Xu, D., Zhang, X., Han, W., McMinn, A., & Ye, N. (2020). Decreased motility of flagellated microalgae long-term acclimated to CO₂-induced acidified waters. *Nature Climate Change*, *10*(6), 561-567. <https://doi.org/10.1038/s41558-020-0776-2>

All content in PEARL is protected by copyright law. Author manuscripts are made available in accordance with publisher policies. Wherever possible please cite the published version using the details provided on the item record or document. In the absence of an open licence (e.g. Creative Commons), permissions for further reuse of content should be sought from the publisher or author.

1 This is the author's accepted manuscript. The final published version of this work (the version of
2 record) is published by Nature in *Nature Climate Change*. The accepted manuscript was made
3 available online on the 1 June 2020 at: doi:[10.1038/s41558-020-0776-2](https://doi.org/10.1038/s41558-020-0776-2) This work is made
4 available online in accordance with the publisher's policies. Please refer to any applicable terms
5 of use of the publisher.

7 **Decreased motility of flagellated microalgae grown in** 8 **CO₂-induced acidified waters for over five years**

9 Yitao Wang^{1,2}, Xiao Fan¹, Guang Gao³, John Beardall^{3,4}, Kazuo Inaba⁵, Jason M. Hall-
10 Spencer^{5,6}, Dong Xu¹, Xiaowen Zhang¹, Wentao Han¹, Andrew McMinn⁷ and Naihao

11 Ye^{1,2*}

12 ¹Yellow Sea Fisheries Research Institute, Chinese Academy of Fishery Sciences, Qingdao, China

13 ²Function Laboratory for Marine Fisheries Science and Food Production Processes, Qingdao
14 National Laboratory for Marine Science and Technology, Qingdao, China

15 ³State Key Laboratory of Marine Environmental Science, Xiamen University, Xiamen 361005,
16 China

17 ⁴School of Biological Sciences, Monash University, Clayton, Victoria 3800, Australia

18 ⁵Shimoda Marine Research Center, University of Tsukuba, Shizuoka, Japan

19 ⁶School of Biological and Marine Sciences, University of Plymouth, PL4 8AA, UK.

20 ⁷Institute of Antarctic and Southern Ocean Studies, University of Tasmania, P.O. Box 252-77,
21 Tasmania 7001, Australia

22 *E-mail: yenh@ysfri.ac.cn

23 Motility plays a critical role in algal survival and reproduction, thus affecting
24 the stability of aquatic ecosystems. However, little is known about the effect of
25 elevated CO₂ in marine, brackish and freshwater systems on algal motility. This
26 study used both laboratory microscale and field mesoscale experiments to
27 investigate the motility of three typical phytoplankton species, polar marine
28 *Microglena* sp., euryhaline *Dunaliella salina* and freshwater *Chlamydomonas*
29 *reinhardtii* grown under different CO₂ concentrations for five years. Motility and
30 the photo-responses of long-term acclimated *Microglena* sp. decreased
31 significantly with increasing CO₂ in all experimental treatments. In a photophobic
32 reaction, changes in intracellular calcium concentration were greatly affected by
33 increasing CO₂. Transcriptomic results showed that genes involved in the
34 regulation of flagellar movement, such as photoreceptor genes, dynein and other
35 axonemal components, were all significantly down-regulated. There was a
36 significant increase in the expression of genes for flagellar shedding under higher
37 CO₂. Parallel experiments with *D. salina* and *C. reinhardtii* showed similar results,
38 suggesting that the observed changes to motility are common across flagellated
39 species. The structure and the bending mechanism of flagella is conserved from
40 unicellular organisms to vertebrates, and thus increases in CO₂ surface water
41 concentrations may affect all flagellated cells exposed to acidified conditions, from
42 algae to fish. Our study suggests that water acidification driven by elevated CO₂
43 may affect survival and reproduction of organisms with flagella and thus alter the
44 structure and diversity of aquatic ecosystems.

45 Marine phytoplankton account for nearly 50% of annual global primary productivity¹.
46 They are the basis of most marine food webs, and provide materials and energy to
47 support complex and productive higher trophic levels². Many phytoplankton migrate
48 vertically on a daily basis to optimize photosynthesis and decrease predation³. For many
49 algae, this motion is achieved by the beating of flagella⁴. Unicellular flagellate algae
50 swim towards light by positive phototaxis but if the light is too strong they use
51 photophobic reaction responses to swim away and avoid damage from strong light
52 (negative phototaxis)^{5,6}.

53 Here we assess the effects of rising CO₂ levels on movement in a range of algae,
54 because about one third of carbon dioxide released into the atmosphere as a result of
55 human activity has been taken up by surface water masses since the Industrial
56 Revolution, with potential effects on flagellated marine biota. When carbon dioxide
57 dissolves in water it lowers the pH potentially affecting the motility of algae^{7,8,9}. Lower
58 pH alters the vertical migration and distribution of *Heterosigma akashiwo*¹⁰, but the
59 effects of CO₂-induced acidification on algal motility are rarely reported, particularly
60 after long-term acclimation.

61 In our study, three flagellated microalgae, representing different taxa, and originating
62 from different aquatic environments (marine/sea ice habitat, estuarine, freshwater),
63 namely *Microglena* sp. from the Antarctic, the widely distributed euryhalophyte
64 *Dunaliella salina* and the freshwater model microalga *Chlamydomonas reinhardtii*,
65 were investigated. We studied changes in cell motility, as measured by positive and
66 negative phototaxis and responses, at different CO₂ concentrations, including

67 preindustrial levels, and linked this to gene expression patterns. *Microglena* sp. was
68 cultured at 280, 400, 700, 1000, 1500 and 2000 ppm CO₂ for 5 years and, over the same
69 period, *C. reinhardtii* and *D. salina* were cultured at 400, 1000 and 2000 ppm. In these
70 experiments, we measured both average and instantaneous velocities, representing the
71 ability of microalgae to search for optimal light intensity and quickly escape predators,
72 respectively. We also carried out a field experiment on *Microglena* sp. using natural
73 sunlight to induce positive/negative phototaxis. We address two questions: first, what
74 is the effect of elevated CO₂ on microalgal motility? Secondly, what are the molecular
75 mechanisms that underpin photoreception and motility at the transcriptome level in
76 response to elevated CO₂? We sequenced the entire genome of *Microglena* sp. and
77 provide results from this marine species in the main paper. Our parallel experiments on
78 the brackish water and freshwater flagellates showed the same responses.

79 As CO₂ levels increased, the average velocity of *Microglena* sp., *C. reinhardtii* and
80 *D. salina* decreased; all the differences were significant at 1000 ppm ($p < 0.05$, Fig. 1a-
81 d, Supplementary Figure 1). Further verification experiments using natural sunlight also
82 showed that the velocity of the algal cells decreased under acidification, and that the
83 decrease was also significant at 1000 ppm ($p < 0.05$, Fig. 1e-h). As shown in
84 Supplementary Figures 2-4, the higher the velocity of the cells, the higher proportion
85 of cell numbers in the movement direction. These results were consistent with the
86 results that are shown in Fig. 1 and Supplementary Figure 1. Measurements of
87 instantaneous velocities also showed similar results to those of average velocities
88 (Supplementary Figures 5-7). Real-time fluorescence images of the cells also reflected

89 the changes in cell velocity under different pCO₂ (Supplementary Figure 8). Elevated
90 pCO₂ had an adverse effect on cell motility (Supplementary Figure 8). Furthermore,
91 the differential roles of seawater pCO₂ and pH on cell motion were studied. The results
92 showed that the decrease of pH resulted in a significant decrease of cell velocity ($p <$
93 0.05 , Supplementary Figures 9a-d, 10a-d, 11a-d) but the increase of CO₂ without a pH
94 shift had no a significant effect on cell velocity ($p > 0.05$, Supplementary Figures 9e-h,
95 10e-h, 11e-h).

96 In the study of positive/negative phototaxis under various CO₂ treatments and
97 different experimental scales, we found that the average velocity of *Microglena* sp., *C.*
98 *reinhardtii* and *D. salina* showed no significant difference between laboratory
99 microscale and field mesoscale experiments ($p > 0.05$, Supplementary Tables 1-5)
100 except for movement of *Microglena* sp. in the vertical direction under 1500 and 2000
101 ppm CO₂ (Supplementary Table 1), wherein the velocity of positive phototaxis was
102 significantly higher than the velocity of negative phototaxis ($p < 0.05$). This may be
103 due to buoyancy induced by O₂ released by photosynthesis as our vertical phototaxis
104 response direction was designed to be bottom-up (Supplementary Figures 12a, 13a,
105 14a).

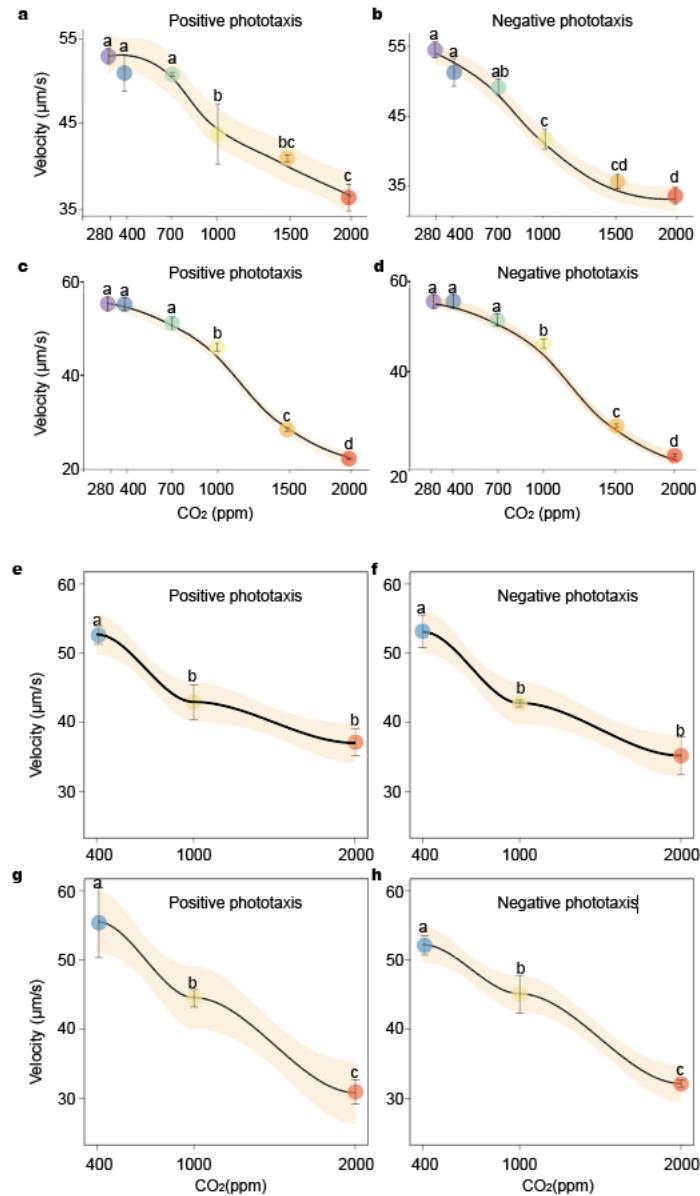
106 The effect of positive/negative phototaxis on instantaneous velocity was striking. The
107 positive phototaxis velocity of *Microglena* sp. was significantly higher than that of the
108 negative phototaxis velocity in the both vertical and horizontal directions, except for
109 the horizontal motion under 400 ppm CO₂ ($p < 0.05$, Supplementary Table 6). The
110 positive phototaxis velocity of *C. reinhardtii* and *D. salina* was also significantly higher

111 than that of the negative phototaxis velocity in the horizontal direction ($p < 0.05$), a
112 result which was similar to that of *Microglena* sp.. However, in the vertical direction,
113 the negative phototaxis velocity of *C. reinhardtii* and *D. salina* was significantly higher
114 than that of the positive phototaxis velocity ($p < 0.05$), except for 2000 ppm treatment
115 of *C. reinhardtii* in the vertical direction (Supplementary Tables 7-8).

116 Our study shows that elevated CO₂ significantly reduced the instantaneous velocity
117 and average velocity of the cells at both laboratory microscale and field mesoscale
118 levels in *Microglena* sp., *C. reinhardtii* and *D. salina* ($p < 0.05$, Fig. 1 and
119 Supplementary Figures 1, 5, 6, 7). Here we report the analyses of algal photoresponse
120 under blue light, but our results were the same using white light or sunlight
121 (Supplementary Figures 15,16, Supplementary Tables 9-12).

122

123



124

125 **Fig. 1 | Average velocity of *Microglena* sp. induced by artificial light and sunlight in the field.**

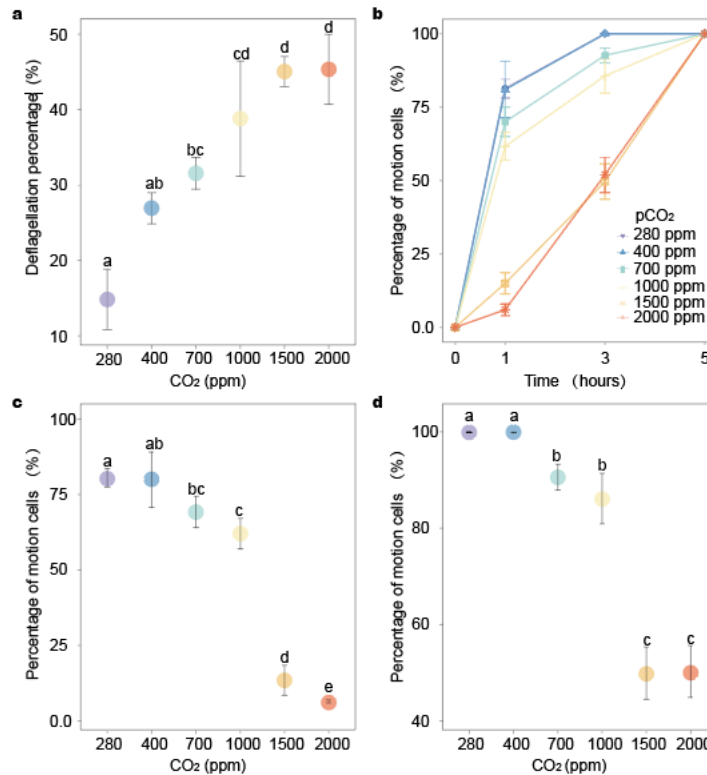
126 **a**, Positive phototaxis induced by white light in the vertical direction. **b**, Negative phototaxis
 127 induced by white light in the vertical direction. **c**, Positive phototaxis induced by white light in the
 128 horizontal direction. **d**, Negative phototaxis induced by white light in the horizontal direction. **e**,
 129 Positive phototaxis in the vertical direction. **f**, Negative phototaxis in the vertical direction. **g**,
 130 Positive phototaxis in the horizontal direction. **h**, Negative phototaxis in the horizontal direction.
 131 Curve fitting was performed by a “loose” method using a `geom_smooth` function in the R
 132 package “`ggplot2`”. The shaded part represents the 95% confidence interval of the fitted curve. Mean
 133 ± SD values per experimental assay are given (n = 3). Different letters in superscript indicate
 134 significant differences (p < 0.05) among treatments.

135 There was a significant increase in deflagellation and a decrease in restoration of

136 motility under CO₂-induced acidification (Fig. 2). Long-term CO₂ treatments led to an

137 increase in the deflagellation ration resulting a decrease in the number of motile cells
138 (Fig. 2a). Increased CO₂ prolonged the recovery time of the proportion of motile cells
139 (Fig. 2b). When CO₂ exceed 1000 ppm, the recovery time of *Microglena* sp. motility
140 was more than 3 hours, significant longer than under 400 ppm ($p < 0.05$, Fig. b-d). This
141 may be related to pH-shock, in which lowering pH induces Ca²⁺-influx and
142 deflagellation¹¹. Non-motile cells without flagella usually sink to the bottom and die
143 under natural conditions^{4,12}. Although *Microglena* sp., *C. reinhardtii* and *D. salina*
144 growth increased with acidification in laboratory conditions (Supplementary Figures
145 17, 18), decreased motility (Fig. 1, Supplementary Figures 1) would likely prove fatal
146 in the natural environment due to a decreased capacity to escape from biotic and abiotic
147 threats. Thus, we predict that under natural conditions, elevated CO₂ will adversely
148 impact the survival of microalgae with flagella.

149



150

151 **Fig. 2 | CO₂ concentration effects on proportion of *Microglena* sp. showing deflagellation and**
 152 **restoration of motility. a, Deflagellation percentage. b, Percentage of motile cells. c, Percentage**
 153 **of motile cells after 1 hour. d, Percentage of motile cells after 3 hour. Mean ± SD values per**
 154 **experimental assay are given (n = 3). Different letters in superscript indicate significant differences**
 155 **(p < 0.05) among treatments.**

156 To clarify the impact of increased CO₂ on flagella, the molecular mechanism by
 157 which acidification causes a decrease in swimming velocity was studied in *Microglena*
 158 sp. (Fig. 3). We focused on 12 flagella bending genes (Supplementary Table 13) that
 159 showed changes in gene expression from transcriptome data and were verified by RT-
 160 PCR. Under long-term acidification, transcriptome data showed that genes of
 161 *Microglena* sp. which are involved in the initial step for Ca²⁺-signaling were all down-
 162 regulated (p < 0.05, Fig. 3f). Genes that promote flagellar motion were all down-
 163 regulated in the 1000 ppm CO₂ treatments compared to those in the 400 ppm treatment
 164 (p < 0.05, Fig. 3d,e). However, CK1 and PKA, which suppress flagellar motion, were
 165 significantly up-regulated (p < 0.05, Fig. 3e). Furthermore, dynein assembly genes,

166 DNAAF3/PF22, were down-regulated and deflagellation genes, DIP13/NA14, were
167 up-regulated ($p < 0.05$, Fig. 3c). DC3, a Ca^{2+} -binding component of the dynein-docking
168 complex involved in the dynein assembly, was highly up-regulated ($p < 0.05$, Fig. 3d).
169 The changes in gene expression pattern on acidification in *Microglena* sp. was not
170 restricted to motility gene but occurred on the whole genome level (Supplementary
171 Figure 19). Real-time imaging showed that intracellular Ca^{2+} concentration during
172 positive phototaxis increased, whereas it decreased during negative phototaxis, when
173 the cells were acclimatized to high CO_2 (Fig. 3g, Supplementary Figure 20). These
174 changes were also observed in *C. reinhardtii* and *D. salina* (Supplementary Figure 21).

175 Given the 5 year length of our experiment, we queried whether genetic modifications
176 had occurred in the algal genome. Illumina WGS was performed for both normal and
177 acidification-treated samples to determine differences in the level of genetic mutations.
178 After mapping c. 240 Gbp reads of normal and acidification-treated samples to the
179 reference genome, it was shown that the overall numbers of SNP (single nucleotide
180 polymorphism) sites were evenly distributed across the genome with a few peaks at
181 specific sites (Supplementary Fig. 22). The normal sample was significantly lower in
182 overall SNPs number compared with the acidified samples (Supplementary Fig. 23). In
183 addition, of all acidified samples, the number of overall SNP sites increased as the CO_2
184 concentration went up (Supplementary Fig. 23), indicating that acidification was highly
185 impacting on the genetic modifications. Focusing on the relationship between genetic
186 modification and flagellum movement, we specifically studied the SNP profiles of 14
187 genes directly related to movement. It can be seen from the Supplementary figure 24

188 that the accumulation of single nucleotide mutations in all the motion-related genes is
189 positively correlated with the degree of acidification ($R^2 \gg 0$). The correlation is
190 significant in 6 of all 14 gene ($P < 0.1$). These genes take their role in motility,
191 phosphorylation and dynein assembly, indicating the genetic adaptation of motility to
192 the oceanic acidification. In order to investigate the effect of genetic mutations on
193 codons, we calculated the synonymous mutation rate and the non-synonymous
194 mutation rate of motion-related genes (Supplementary Figure 25). We found K_a are
195 generally less than K_s when compared in 400 ppm ($p < 0.05$), indicating more mutations
196 do not cause changes in the coding protein in the normal acidification. However, the
197 difference does not exist in 1000 ppm and 2000 ppm. This indicates that with the
198 increase of acidification gradient, more non-synonymous mutations will occur, thus
199 accelerating the selection effect of environment on individual genes. This conjecture is
200 supported somewhat by another diagram. We found that the median value of K_a/K_s
201 climb as acidification increased, however it is not significant.

202

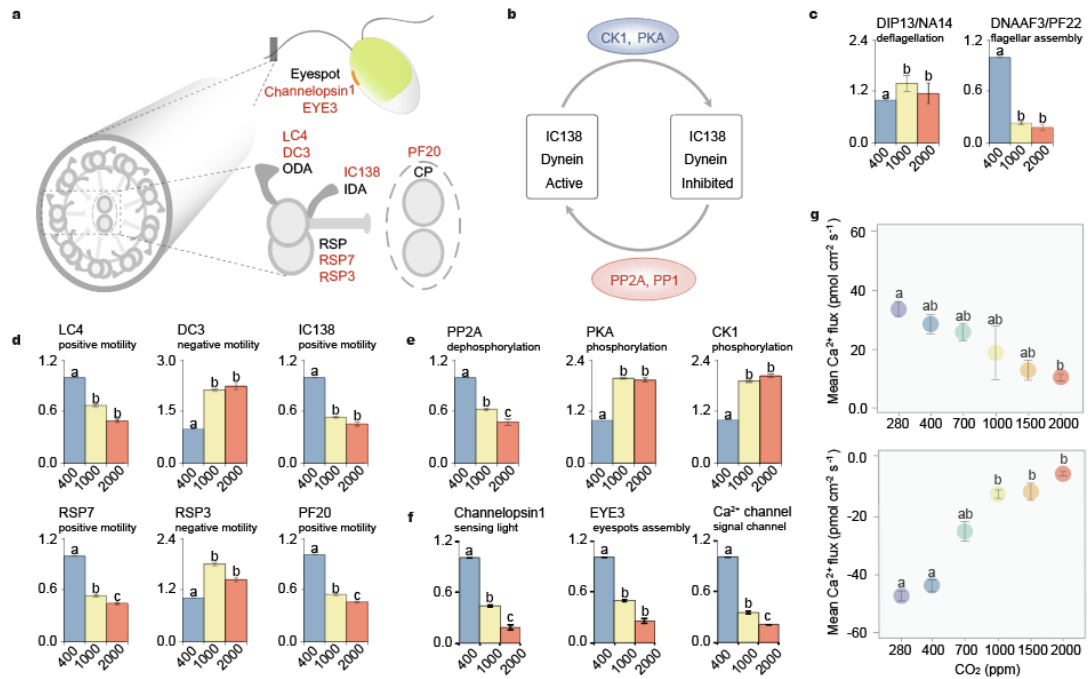


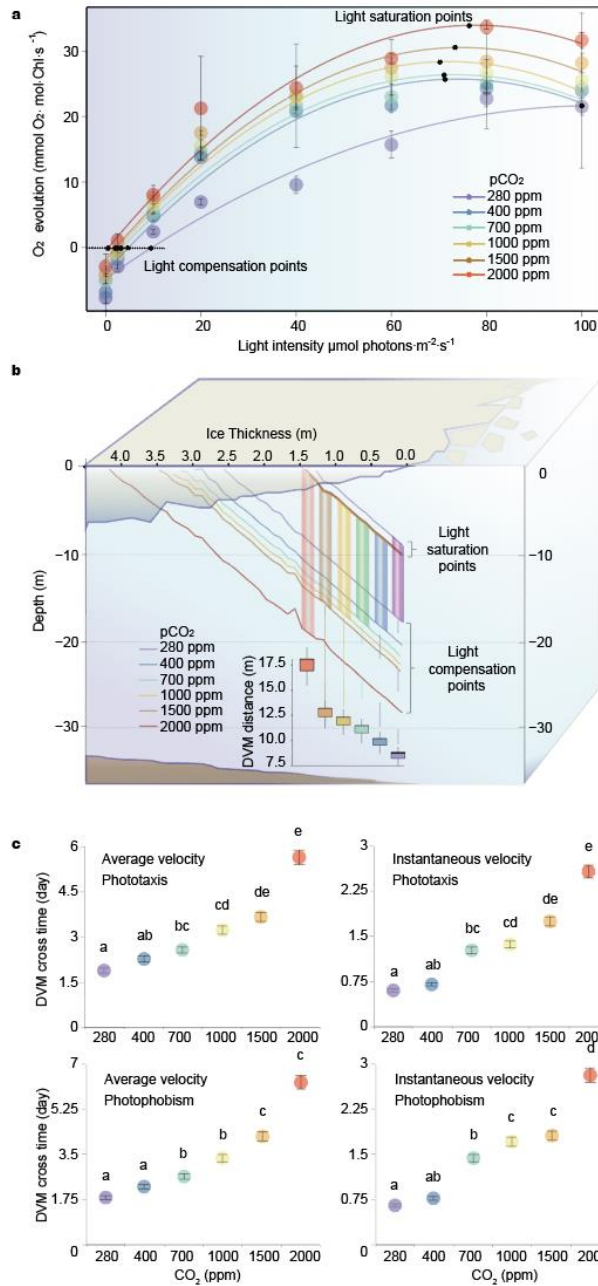
Fig. 3 | Changes in the expression of motility-related genes. **a**, Schematic diagram of light sensation and Ca^{2+} - mediated flagellar beating in *Microglena* sp.. ODA, outer dynein arm. IDA, inner dynein arm. RSP, radial spoke protein. CP, central pair apparatus. The genes for RT-PCR are listed in red. **b**, Regulation of an inner dynein arm by the phosphorylation/dephosphorylation of IC138 via protein kinases and phosphatases. **c**, Changes of gene expression for deflagellation and flagellar assembly under the 1000 and 2000 ppm treatments relative to the 400 ppm treatment. **d**, Changes of gene expression for dynein subunits under the 1000 and 2000 ppm treatments relative to the 400 ppm treatment. **e**, Changes of gene expression for the regulation of IC138 under the 1000 and 2000 ppm treatments relative to the 400ppm treatment. **f**, Changes of gene expression for eye-spot and Ca^{2+} -regulation under the 1000 and 2000 ppm treatments relative to the 400ppm treatment. **g**, the mean flux of Ca^{2+} under different p CO_2 scenarios. Mean \pm SD values per experimental assay are given (n = 3). Upper, Ca^{2+} efflux under positive phototaxis. Lower, Ca^{2+} influx under negative phototaxis, “-” on the vertical scale means Ca^{2+} entry. LC4, flagellar outer dynein arm light chain 4; DC3, outer dynein arm docking complex protein 3; IC138, a 138 kDa intermediate chain of I1/f inner arm dynein; RSP, radial spoke protein; PF20, a protein of the central pair apparatus; PKA, cAMP-dependent protein kinase; PP2A, protein phosphatase 2A; CK1, casein kinase 1; DIP13/NA14, deflagellation inducible protein; DNAAF3/PF22, axonemal dynein assembly factor. Mean \pm SD values per experimental assay are given (n = 3). Different letters in superscript indicate significant differences (p < 0.05) among treatments.

The phototactic pathway of *Microglena* sp. is not fully understood. Due to the highly-conserved structure of the flagellum and similarity of photosensitive organs of flagellated green microalgae, *C. reinhardtii* was used to annotate flagellate-related genes in the *Microglena* sp. motility-related genes, so the existing *C. reinhardtii*

227 pathway was used to study the *Microglena* sp. motility-related genes. The phototactic
228 pathway of *Chlamydomonas* primarily consists of three steps: (i) a light inward current
229 in the eyespot, which functions as a light reflector and light-gated ion channel¹¹. (ii) a
230 photocurrent depolarized activated voltage-gated Ca²⁺ channel in flagella^{5,11,13}. (iii)
231 flagellar bending stimulated by Ca²⁺ and inhibited by cAMP⁵. Flagellar beat is driven
232 by the axonemal dyneins, which are regulated by Ca²⁺ -binding proteins LC4, DC3¹¹
233 and a phosphorylation protein IC138. The components of radial spokes and central pair
234 apparatus also play a significant role in regulating axonemal dyneins^{5,11,13,14,15}. The
235 present study shows that long-term acidification negatively affected expression of
236 genes related to photosensitivity, signal transduction and the regulation of dyneins and
237 flagellar motility (Fig. 3). In addition, the acidification resulted in decreased formation
238 and stability of flagella (Fig. 3c). Taken together, these results suggest that long-term
239 exposure to acidification has negative effects on the motility of *Microglena* sp..
240 Under the business as usual emissions scenario (RCP8.5, IPCC 2019), Antarctic
241 terrestrial ice-free areas could increase by close to 25% by the end of the century,
242 causing fundamental changes to the region¹⁶. Changes in phytoplankton species
243 composition and the seasonality of production affect Antarctic food webs and are
244 induced by the retreat of winter sea ice¹⁷. As a polar alga, *Microglena* sp. will be
245 affected by both sea ice loss and acidification, since its light compensation point is
246 reduced under ocean acidification (Fig. 4a).

247 *Microglena* sp. survives under sea ice all year round¹⁸. Due to the strong attenuation
248 of natural light through the ice, light intensity under the ice is much lower than in non-

249 ice-covered waters⁹ and *Microglena* sp. is well adapted to an under-ice, low light
250 environment¹⁸. When sea ice melts, accelerated by climate change, *Microglena* sp. is
251 exposed to much greater light intensities. Consequently, the vertical migration distance
252 increases if cells are to position themselves in a region of appropriate light intensity
253 (Fig. 4). As shown in Fig. 4c, we calculated how much time it would take *Microglena*
254 sp. to cover the DVM using the average and instantaneous velocities under
255 positive/negative phototactic responses. Under positive phototaxis, at 2000 ppm, the
256 average velocity is 0.13 m/h and the instantaneous velocity is 0.29 m/h. It would take
257 *Microglena* sp. 2.57-5.65 days to cross the DVM. For *Microglena* sp. adapted to 280
258 ppm, it would take 14.64 h, to 1.89 days. It also takes show an extended period of time
259 to cross the DVM under increased CO₂ during the negative phototaxis response.
260 However, an increase in ocean acidification will decrease the motility of *Microglena*
261 sp., which we suspect will put this organism at a disadvantage such that it will likely be
262 outcompeted in ice-free conditions, changing the Antarctic ecosystem. *C. reinhardtii*
263 and *D. salina*, which are not protected by ice, experience dramatic changes in the light
264 in their environment. In this case, the cells can escape light stress through motility.
265 Prolonged exposure to bright light increases the risk of light damage and increasing
266 CO₂ concentrations decreased cells motility, which can lead to prolonged exposure to
267 high light stress and thus increase the risk of photo-damage. At the same time,
268 weakened motility will make it harder for cells to escape predators^{4,12}.



269

270 **Fig. 4 | Distribution of *Microglena* sp. and light intensity under melting ice.** **a**, Photosynthetic
 271 light curve of *Microglena* sp. under different CO₂ concentrations. Mean ± SD values per
 272 experimental assay are given (n = 3). **b**, The incident light distribution in the water under melting
 273 ice. Upper and lower horizontal lines represent saturating light intensity and the light compensation
 274 point respectively. *Microglena* sp. lives between the saturated and compensation isophotic lines and
 275 moves corresponding to the solar cycle. *Microglena* sp. Daily Vertical Migration (DVM) distance
 276 was defined as the vertical distance between the water layer where the light compensation point of
 277 algae was located and the water layer where the saturation point was located. **c**, *Microglena* sp.
 278 cover the DVM time using the average and instantaneous velocities under positive and negative
 279 phototaxis. Upper left, positive phototaxis using average velocity. Upper right, positive phototaxis
 280 using instantaneous velocity. Lower left, negative phototaxis using average velocity. Lower right,
 281 negative phototaxis using instantaneous velocity.

282 There is growing concern for how biodiversity loss due to human-induced
283 environmental change will affect the functioning of ecosystems and, in turn, the
284 services ecosystems provide to human beings^{19,20}. The influence of elevated pCO₂ on
285 the species biodiversity and richness of the phytoplankton assemblages could be
286 profound, through negative effects on some organisms and changes to biogenic habitat²¹.
287 Our study shows, both at physiological and gene-expression levels, that elevated CO₂
288 concentration significantly decreases the motility of three typical microalgae after a
289 five-year acclimation, which would impact their reproduction and survival, and thus the
290 abundance of microalgae with flagella in aquatic ecosystem. Given that the structure
291 and motility regulation of eukaryotic cilia and flagella are evolutionary conserved^{6,22,23},
292 our study reveals the potential effects of aquatic acidification on a wide range of cilia
293 and flagella in eukaryotic organisms, including sperm motility and fertilization¹², cilia-
294 based epithelial fluid flow and the determination of left–right asymmetry⁶.

295

296 REFERENCES

- 297 1. Field, C. B., Behrenfeld, M. J., Randerson, J. T., & Falkowski, P. Primary production of the
298 biosphere: integrating terrestrial and oceanic components. *Science* **281**, 237-240 (1998).
- 299 2. Ullah, H., Nagelkerken, I., Goldenberg, S.U. & Fordham, D.A. Climate change could drive
300 marine food web collapse through altered trophic flows and cyanobacterial proliferation. *PLOS*
301 *Biol.* **16**, e2003446 (2018).
- 302 3. Hall, N.S. & Paerl, H.W. Vertical migration patterns of phytoflagellates in relation to light and
303 nutrient availability in a shallow microtidal estuary. *Mar. Ecol. Prog. Ser.* **425**, 7-21 (2015).
- 304 4. Stocker, R. & Durham, W.M. Tumbling for Stealth? *Science* **325**, 400-402 (2009).
- 305 5. Sineshchekov, O.A., K.H. Jung, & Spudich, J.L. Two rhodopsins mediate phototaxis to low- and
306 high-intensity light in *Chlamydomonas reinhardtii*. *P. Natl. Acad. Sci. USA* **99**, 8689-8694
307 (2002).
- 308 6. Elgeti, J. Winkler, R.G. & Gompper, G. Physics of microswimmers—single particle motion and
309 collective behavior: a review. *Rep. Prog. Phys.* **78**, 1-50 (2015).
- 310 7. Caldeira, K. & Wickett M.E. Anthropogenic carbon and ocean pH. *Nature* **425**, 365 (2003).

- 311 8. Flynn, K.J., Blackford, J.C., Baird, M.E., Raven, J.A., Clark, D.R., Beardall, J., Brownlee, C.,
312 Fabian, H., & Wheeler, G.L. Changes in pH at the exterior surface of plankton with ocean
313 acidification. *Nat. Clim. Change* **2**, 510-513 (2012).
- 314 9. Assmy, P., Fernández-Méndez, M., Duarte, P. & Meyer, A. Leads in Arctic pack ice enable early
315 phytoplankton blooms below snow-covered sea ice. *Sci. Rep-UK* **7**, 40850 (2017).
- 316 10. Kim, H., Spivack, A.J. & Menden-Deuer S. pH alters the swimming behaviors of the
317 raphidophyte *Heterosigma akashiwo*: Implications for bloom formation in an acidified ocean.
318 *Harmful Algae* **26**, 1-11 (2013).
- 319 11. Wheeler, G.L. Calcium-Dependent signalling processes in *Chlamydomonas*. *Chlamydomonas:*
320 *Molecular Genetics and Physiology*. (eds Hippler, M.) 233-255 (Springer, Cham, Heidelberg
321 2017).
- 322 12. Waisbord, N. & Guasto, J.S. Peculiar polygonal paths. *Nat. Phys.* **14**, 1157-1162 (2018).
- 323 13. Uekia, N. & Wakabayashi, K. Detergent-extracted *Volvox* model exhibits an anterior–posterior
324 gradient in flagellar Ca²⁺ sensitivity. *P. Natl. Acad. Sci. USA* **115**, E1061-E1068 (2018).
- 325 14. Yang, X.L., Xu, H., Li, D., Gao, X., Li, T.L. & Wang, R. Effect of melatonin priming on
326 photosynthetic capacity of tomato leaves under low-temperature stress. *Photosynthetica* **56**,
327 884-892 (2018).
- 328 15. Indaba, K. Sperm flagella: comparative and phylogenetic perspectives of protein components.
329 *MHR: Basic Sci. of Reprod. Med.* **17**, 524-538 (2011)
- 330 16. Shikata, T., Matsunaga, S., Nishide, H., Sakamoto, S., Onistuka, G. & Yamaguchi, M. Diurnal
331 vertical migration rhythms and their photoresponse in four phytoflagellates causing harmful
332 algal blooms. *Limnol. Oceanogr.* **60**, 1251-1264 (2015).
- 333 17. Smetacek, V. & Nicol, S. Polar ocean ecosystems in a changing world. *Nature* **437**, 362-368
334 (2005).
- 335 18. Raymond, J.A. & Morgan-Kiss, R. Multiple ice-binding proteins of probable prokaryotic origin
336 in an Antarctic lake alga, *Chlamydomonas* sp. ice-mdv (Chlorophyceae). *J. Phycol.* **53**, 848–854
337 (2017).
- 338 19. Duffy, J.E., Godwin, C.M. & Cardinale, B. J. Biodiversity effects in the wild are common and
339 as strong as key drivers of productivity. *Nature* **549**, 261 (2017).
- 340 20. Hall-Spencer, J. M., & Harvey, B. P. Ocean acidification impacts on coastal ecosystem services
341 due to habitat degradation. *Emerg. Top. in Life Sci.*, **3**, 197-206 (2019).
- 342 21. Sunday, J.M., Fabricius, K.E., Kroeker, K.J. & Anderson, K.M. Ocean acidification can mediate
343 biodiversity shifts by changing biogenic habitat. *Nat. Clim. Change* **7**, 81 (2017).
- 344 22. Jeanneret, R., Contino, M. & Polin M. A brief introduction to the model microswimmer
345 *Chlamydomonas reinhardtii*. *Eur. Phys. J. Spec. Top.* **225**, 2141-2156 (2016).
- 346 23. Indaba, K. & Mizuno, K. Sperm dysfunction and ciliopathy. *Reprod. Med. Biol.* **15**, 77-94 (2016).
- 347 24. Platt, T., Gallagos, C.C. & Hamson, W. G. Photoinhibition of photosynthesis in natural
348 assemblages of marine phytoplankton. *J. Mar Res.* **38**, 687-701 (1980).
- 349 25. Li, Y., Horsman, M., Wang, B., Wu, N., & Lan, C. Q. Effects of nitrogen sources on cell growth
350 and lipid accumulation of green alga *Neochloris oleoabundans*. *Appl. Microbial. Biot.*, **81**, 629-
351 636 (2008).
- 352 26. Lichtenthaler, H.K. Chlorophylls and Carotenoids: Pigments of Photosynthetic Biomembranes.
353 *Method. Enzymo.* **148**, 350-382 (1987).
- 354 27. Sueltemeyer, D.F., Klug, K. & Fock, H.P. Effect of photon fluence rate on oxygen evolution and

- 355 uptake by *Chlamydomonas reinhardtii* suspensions grown in ambient and CO₂-enriched air.
356 *Plant Physiol.* **81**, 372-375 (1986).
- 357 28. Rühle, T., Hemschemeier, A., Melis, A. & Happe, T. A novel screening protocol for the isolation
358 of hydrogen producing *Chlamydomonas reinhardtii* strains. *BMC Plant Biol.* **8**, 107 (2008).
- 359 29. Siiltemeyer, D.F., Klock, G., Kreuzberg, K. & Fock, H.P. Photosynthesis and apparent affinity
360 for dissolved inorganic carbon by cells and chloroplasts of *Chlamydomonas reinhardtii* grown
361 at high and low CO₂ concentrations. *Planta* **176**, 256-260 (1988).
- 362 30. Ueki, N., Ide, T., Mochiji, S., Kobayashi, Y. & Tokutsu, R. Eyespot-dependent determination of
363 the phototactic sign in *Chlamydomonas reinhardtii*. *P. Natl. Acad. Sci. USA* **113**, 5299-5304
364 (2016).
- 365 30. SooHoo, J.B., Palmisano, A.C., Kottmeier, S.T., Lizotte, M., SooHoo, S.L. & Sullivan, C.
366 Spectral light absorption and quantum yield of photosynthesis in sea ice microalgae and a bloom
367 of *Phaeocystis pouchetii*. *Mar. Ecol-Prog. Ser.* **39**, 175-189 (1987).
- 368 31. Sun, J., Wang, M.J., Ding, M.Q., Deng, S.R., Liu, M.Q., Lu, C.F., Zhou, X.Y., Shen, X., Zheng,
369 X.J., Zhang, Z.K., Song, J., Hu, Z.M., Xu Y. & Chen S.L. H₂O₂ and cytosolic Ca²⁺ signals
370 triggered by the PMH⁺-coupled transport system mediate K⁺/Na⁺ homeostasis in NaCl-stressed
371 *Populus euphratica* cells. *Plant Cell Environ.* **33**, 943-958 (2010).

372

373 **Acknowledgements** This work was supported by the national key re-search and development
374 program of China (2018YFD0900703, 2016YFC1402102, 2018YFD0901503-8), Marine S&T
375 Fund of Shandong Province for Pilot National Laboratory for Marine Science and Technology
376 (Qingdao) (NO. 2018SDKJ0406-3); Financial Fund of the Ministry of Agriculture and Rural Affairs,
377 P. R. of China (NFZX2018). Projects of International Exchange and Cooperation in Agriculture,
378 Ministry of Agriculture and Rural Affairs of China- Science, Technology and Innovation
379 Cooperation in Aquaculture with Tropical Countries along the Belt and Road; Shandong key
380 Research and Development Plan (2018GHY115010); National Natural Science Foundation of China
381 (41676145); China Agriculture Research System (CARS-50); Central Public-interest Scientific
382 Institution Basal Research Fund, YSFRI, CAFS (20603022016001, 20603022019006); Taishan
383 Scholars Funding of Shandong Province; Talent Projects of Distinguished Scientific Scholars in
384 Agriculture.

385 **Author contributions** N.H.Y. designed the project. Y.T.W., D.X., X.W.Z. and W.T.H performed the
386 research. F.X., N.H.Y., and Y.T.W. analyzed the data. Y.T.W. and N.H.Y. wrote the first draft and all
387 authors contributed to interpreting the data and writing the manuscript. The authors declare no
388 conflict of interest.

389 **METHODS**

390 **Cell Culture.** *Microglena* sp., *Chlamydomonas reinhardtii* and *Dunaliella salina* acquired from
391 Yellow Sea Fisheries Research Institute were used in this study. These three species were semi-
392 continuously cultured in aerated 500 ml conical flasks containing 400 ml of medium
393 (Supplementary Table 2, 3, 4) in a 12-h/12-h light/dark cycle and at 6°C, 20°C, 20°C, respectively.

394 *Microglena* sp. was cultured in a series of CO₂ treatments (280, 400, 700, 1000, 1500, 2000 ppm),
395 coded as “M₂₈₀”, “M₄₀₀”, “M₇₀₀”, “M₁₀₀₀”, “M₁₅₀₀”, “M₂₀₀₀”, respectively. *C. reinhardtii* was
396 cultured in three CO₂ treatments (400, 1000, 2000 ppm), coded as “CR₄₀₀”, “CR₁₀₀₀”, “CR₂₀₀₀”,

397 respectively. *D. salina* was also cultured in three CO₂ treatments (400, 1000, 2000 ppm) coded as
398 “DS₄₀₀”, “DS₁₀₀₀”, “DS₂₀₀₀”, respectively. The ambient CO₂ concentration of 400 ppm was
399 designated the control treatment. All cultures (Supplementary Table 14-16) were conducted in CO₂
400 plant incubators (HP-1000, Ruihua, China) to maintain the stability of CO₂ and the variations of
401 CO₂ was shown in Supplementary Tables 17-20. The pH in each culture was monitored once every
402 day using a portable pH electrode (6010M, Jenco, USA) to ensure the stability of the pH level during
403 the culture period (Supplementary Tables 17-18). All following experiment assays were performed
404 using cells in the light period (6~8 h after the light came on) after the five-year acclimation.

405 **Photosynthesis vs light curve.** For each sample, oxygen production and oxygen uptake were
406 obtained at 6 °C using 4 mL respiration chambers fitted with micro-probes, glass-coated stir bars,
407 Clark-type OX-MR oxygen microsensors and a PA 2000 picoammeter, and data logged using MicOx
408 2.6 data acquisition software (Microrespiration system, Unisense). Oxygen microsensors were
409 polarized continuously for > 24 hours before use. Oxygen production and oxygen uptake ratio were
410 recorded at different light intensities using LEDs and then fitted to the relationships described by
411 Platt *et al.* (1980)²⁴ (Supplementary Table 21). The intersection point between the photosynthetic
412 oxygen release curve and the X-axis is the light compensation point, and the point when the
413 photosynthetic oxygen release reaches its maximum value is the light saturation point.

414 **Chlorophyll determination.** Chlorophyll measurement Fresh algal cells collected in a 2ml
415 centrifuge tube from 2ml cultivated broth by centrifuge were disrupted in an ultrasonic bath
416 (KQ3200DA, Kunshan, China) in ice bath for 45 min and extracted with 2 ml 95% ethanol overnight

417 in 4°C. The extractant was centrifuged at 3,000×g for 5 min²⁵. The chlorophyll content was
418 determined spectrophotometrically as follows:

419 $\text{Chl} = 5.24A_{664.2} + 22.24A_{648.6}$, where $A_{664.2}$ and $A_{648.6}$ represent absorbance of the methanol extracts
420 at 664.2 and 648.6 nm, respectively²⁶.

421 **Light intensity for positive and negative phototaxis.** Phototaxis is the biological tendency to
422 move under light stimulation. Positive phototaxis occurs when algae sense light through the eyespot
423 and move toward it through their motor organs. Negative phototaxis is a reaction of algae to sense
424 light through the eyespot and away from it through their motor organs. Compared with *C. reinhardtii*,
425 *Microglena* sp. had a very low light compensation point (4.8 μmol photons·m⁻²·s⁻¹) and saturation
426 points (73.82 μmol photons·m⁻²·s⁻¹), which is about 10% that of *C. reinhardtii* under normal
427 conditions (Fig. 4a). Light density distribution with variations in incident irradiance were measured
428 during the positive/negative phototaxis assays of *Microglena* sp., *C. reinhardtii* and *D. salina*
429 (Supplementary Figure 12, 13). Consequently, irradiances of 2 μmol photons·m⁻²·s⁻¹ and 200 μmol
430 photons·m⁻²·s⁻¹ were selected as the positive phototaxis-inducing light and negative phototaxis-
431 inducing light respectively. For *C. reinhardtii* and *D. salina*, the positive phototaxis-inducing light
432 was the same as that induced by *Microglena* sp. and negative phototaxis-inducing light was 800
433 μmol photons·m⁻²·s⁻¹ 27-29.

434 **Vertical cell motion.** Cells were washed with pre-acidified experimental solution with different
435 pCO₂ and kept under red light for more than 50 min before the assays³⁰. In all the experiments
436 involving light induction, we use a customized LED light source with multiple lamp beads, which
437 can emit parallel light of wavelengths of 400-700 nm and with the light intensity adjustable in the
438 range of 0-2000 μmol photons·m⁻²·s⁻¹. For vertical laboratory microscale experiments, the acrylic
439 channel used had an inner diameter of 4.4 cm and a height of 11 cm (Supplementary Figure 12a,

440 14a). In order to maintain the stability of the acrylic channel, in the outdoor experiment, we extended
441 the length of the acrylic channel to 40 cm and used only the top 11 cm during mesoscale experiments
442 (Supplementary Figure 13a). For the positive phototaxis assays, 15 mL cell suspensions ($\sim 2.4 \times 10^6$
443 cells/mL) were placed into the bottom of acrylic channels by a pipette, illuminated with a LED
444 (White/Blue, $\sim 2 \mu\text{mol photons} \cdot \text{m}^{-2} \cdot \text{s}^{-1}$) from immediately above for 20 min and sampled every
445 centimeter (Supplementary Figures 14a). For the negative phototaxis assays, 15 mL cell suspensions
446 ($\sim 2.4 \times 10^6$ cells/mL) were placed into the top of the acrylic channels by a pipette, illuminated with
447 a LED (White/Blue, $\sim 200 \mu\text{mol photons} \cdot \text{m}^{-2} \cdot \text{s}^{-1} / \sim 800 \mu\text{mol photons} \cdot \text{m}^{-2} \cdot \text{s}^{-1}$) from immediately
448 above for 20 min, and sampled every centimeter (Supplementary Figures 14a). The positive
449 phototaxis assay treatment was used to keep cells at the top of the vessel during the negative
450 phototaxis assays. To calculate the cell velocity, we chose the average distance from the sampling
451 point to the loading point (as a point without volume) as the distance of the cells had moved at each
452 sampling point. The distance moved was set to 0.5, 1.5, 2.5, 3.5, 4.5, 5.5, 6.5, 7.5, 8.5, 9.5 cm
453 corresponding to samples from 1 to 10, respectively. The average velocity was calculated as follows:
454 Velocity = $(C_1 V_1 x S_1 + C_2 x V_2 x S_2 + \dots + C_{10} x V_{10} x S_{10}) / t / (C_1 x V_1 + C_2 x V_2 + \dots + C_{10} x V_{10})$
455 (Equation 1)

456 C: cell concentration; V: sample volume; S: distance moved; t: move time.

457 **Horizontal cell motion.** Cells were washed with a pre-acidified experimental solution with different
458 CO_2 concentrations and kept under red light for more than 50 min before the assays. For horizontal
459 laboratory microscale experiments, the acrylic channel was oblong with a square cross section with
460 each side being 4 cm, and channels were evenly divided into 11 parts with a width of 1 cm each
461 (Supplementary Figure 12b, 14b). As for the vertical cell motion study, in order to maintain the
462 stability of the acrylic channel, in the outdoor experiment, we extended the length of the acrylic
463 channel to 40 cm and used 11 cm on one end during mesoscale experiments (Supplementary Figure
464 13d). For the positive phototaxis assays, 15 mL cell suspensions ($\sim 2.4 \times 10^6$ cells/mL) were placed
465 into one side of the acrylic channels, matching acrylic cards were inserted to separate the cell
466 suspensions after illuminating with a LED (White, $\sim 2 \mu\text{mol photons} \cdot \text{m}^{-2} \cdot \text{s}^{-1}$) from the opposite side
467 for 20 min and sampled every centimeter (Supplementary Figures 14b). For the negative phototaxis
468 assays, 15 mL cell suspensions ($\sim 2.4 \times 10^6$ cells/mL) were placed into one side of acrylic channels,
469 illuminated with a LED (White, $\sim 200 \mu\text{mol photons} \cdot \text{m}^{-2} \cdot \text{s}^{-1} / \sim 800 \mu\text{mol photons} \cdot \text{m}^{-2} \cdot \text{s}^{-1}$) from side
470 for 20 min, and sampled every centimeter (Supplementary Figures 14b). To calculate the cell
471 velocity, we chose the average distance from the sampling point to the loading point (as a point
472 without volume) as the distance of the cells at each sampling point. The distance moved was set to
473 0.5, 1.5, 2.5, 3.5, 4.5, 5.5, 6.5, 7.5, 8.5, 9.5 cm corresponding to samples from 1 to 10, respectively.
474 The average velocity was calculated as in Equation 1.

475 **Field experiment.** To further study the effect of ocean acidification on algal motion in a more
476 natural ocean setting, we investigated the average velocity of *Microglena* sp. induced by sunlight in
477 a calm bay (Supplementary Figures 13). The horizontal and vertical sampling methods were
478 consistent with the laboratory experiment, but the channel length was increased to 40 cm to ensure
479 the stability of the equipment in seawater. The vertical channels were divided into two parts by
480 rubber plug, the front part is 11 cm, the back part is 29 cm, and the latter part was injected with
481 natural seawater to keep the tank stable. The horizontal channels were divided into two sections by
482 acrylic spacers, the first section is 11 cm, the second section is 29 cm, and the latter section was
483 injected with natural seawater to keep the tank stable. In our experiment, we only used the front-

484 end 11 cm.

485 **Flagellum shedding and regeneration.** *Microglena* sp. was cultured to the exponential growth
486 stage at the different pH values and then aeration was stopped. We used a Nikon Eclipse 80i
487 microscope (Carl Zeiss, Inc., Thornwood, NY) to look at the flagella and calculated the percent of
488 cells without flagella compared to total cells. pH-shocked cells were obtained by rapidly adding a
489 large amount of culture medium saturated with CO₂ to the culture medium containing motile cells,
490 centrifugation was conducted and medium with different acidification gradients was added. The
491 proportion of flagellar regeneration was calculated by recording the motility of the cells.

492 **Transcriptome.** To explore the mechanism by which *Microglena* sp. responds to ocean acidification,
493 on year 5 of the long-term experiment, the cultures of *Microglena* sp. “M400” and “M1000” were
494 selected, centrifuged at 6 °C frozen in liquid nitrogen and stored at -80°C for subsequent
495 transcriptomic (with three biological replicates for each sample) analysis. In order to avoid circadian
496 bias, our sampling time was 6 hours after illumination, i.e. 14:00 h for all samples.

497 **RT-PCR.** RNA isolated from *Microglena* sp. (M400, M1000 and M2000) was treated with DNase
498 I and then reverse-transcribed to cDNA using random hexamers. PCR was then performed using
499 cDNA templates and primers specific for *Microglena* sp. genes MigICE16000, MigICE12547,
500 MigICE10361, MigICE11569, MigICE4581, MigICE14893, MigICE8486, MigICE16283,
501 MigICE4131, MigICE16837, MigICE5195, MigICE9498, MigICE14891, MigICE16200. Control
502 PCR reactions were performed using chromosomal DNA templates and the same primer sets under
503 the same PCR conditions. In order to avoid circadian bias, our sampling time was 6 hours after
504 illumination, i.e. 14:00 h for all samples.

505 **Calcium ions flux measurements.** The net flux of Ca²⁺ between intracellular and extracellular was
506 measured non-invasively using the scanning ion-selective electrode technique (SIET) (the SIET
507 system, BIO-001A, Younger USA Sci. & Tech. Corp., Applicable Electronics Inc. and Science
508 Wares Inc.). The measurements of the Ca²⁺ flux was performed as described by Sun *et al.* (2010)
509 with some modifications³¹. The *Microglena* sp. cells were settled on the center of a poly-L-lysine-
510 pre-treated cover slip and then placed in 4 ml of measuring solution (0.2 mM CaCl₂, 360 mM NaCl,
511 2.0 mM NaHCO₃, 8.0 mM KCl, 0.1 mM Na₂SO₄, 0.05 mM H₃BO₃, 0.5 mM NH₄NO₃, 2.0 mM Tris).
512 Solution was pre-acidified at the corresponding pCO₂ before Ca²⁺ flux measurements. Three-
513 dimensional ionic flux signals were continuously recorded for 5 min and plotted with MageFlux
514 software that was developed by Xu Yue (<http://xuyue.net/mageflux>).

515 **Distribution of *Microglena* sp. distribution and irradiance at different depths under melting**
516 **ice.** *Microglena* sp. live in the seawater beneath sea ice. Light intensity at the boundary of ice water
517 increased to increase with the increase of external light intensity. When the light intensity exceeded
518 the *Microglena* sp. saturation point, the algae moved downward to escape the strong light. When
519 the light is lower than compensation point, the algae move upward to find the appropriate light
520 intensity. We define the distance between compensation point and saturation point as distance of
521 diurnal vertical movement (DVM). During a light cycle, *Microglena* sp. move up and down in
522 seawater within the DVM. Light levels, which were attenuated by sea ice, were obtained from the
523 formula $T=e^{-kb}$, T, extinction coefficient; e, Napierian base; k, constant; b, optical path³². The
524 intensity of light decreases gradually with the thickness of sea ice due to the attenuation effect of
525 sea ice on light. Light levels in sea water were obtained using data that we measured in the North
526 Yellow Sea in October. Sea ice used in this experiment was artificially made from cold storage.
527 After the natural seawater was filtered, the salinity was adjusted to 5 practical salinity units with

528 deionized water, and the temperature was lowered to -15 °C to obtain sea ice of different thicknesses.

529 **Instantaneous velocity.** Measurement of cell instantaneous velocity was based on the modified
530 method of previous studies^{30,32} using particle image velocimetry (PIV) (Stereo-PIV, TSI, USA)^{30,32}.

531 The container (side length 10 cm, opening above) was illuminated from one side by a laser sheet
532 with a wavelength of 532 nm (the light that records the movement of cells). Phototactic responses
533 of the cells were observed when the container was illuminated by LED light (SRZ-BLTO9W-01,
534 GeShuo, China) from the top or side. The light intensity of light was 2 and 200 $\mu\text{mol photons}\cdot\text{m}^{-2}\cdot\text{s}^{-1}$
535 ¹ at the top and side surface of the suspension. The illumination was slightly reduced as the depth
536 within the vessel increased. In order to avoid the slightly non-uniform illumination effect, the
537 brightness of the image at the same depth for the PIV analysis was measured. For *C. reinhardtii* and
538 *D. salina*, the positive phototaxis-inducing light was 2 $\mu\text{mol photons}\cdot\text{m}^{-2}\cdot\text{s}^{-1}$ and negative
539 phototaxis-inducing light was 800 $\mu\text{mol photons}\cdot\text{m}^{-2}\cdot\text{s}^{-1}$.

540 The instantaneous velocity was calculated as follows:

541 $\text{Velocity} = S / t$ (Equation 2)

542 S: displacement; t: move time = 1 s.

543 **Statistical analyses.** Each result that is shown is the mean of at least three biological replicates.

544 Statistical analyses were performed using SPSS v.22 for Windows (SPSS, Chicago, IL, USA).

545 Variance among treatments was tested using Kruskal Wallis test followed by Dunn's post-hoc test.

546 The significance level was $P < 0.05$ for all tests unless otherwise state.

547